IOP Publishing | International Atomic Energy Agency Nuclear Fusion

Nucl. Fusion **61** (2021) 106038 (7pp) https://doi.org/10.1088/1741-4326/ac1e5f

Simulation of equilibrium and transport in advanced FRCS

S.A. Dettrick[1,*], D.C. Barnes[1], F. Ceccherini[1], L. Galeotti[1], S.A. Galkin[1], S. Gupta[1], K. Hubbard[1], O. Koshkarov[1], C.K. Lau[1], Y. Mok[1], A. Necas[1], B.S. Nicks[1], M. Onofri[1], J. Park[1], S.V. Putvinski[1], L.C. Steinhauer[1], K. Yakymenko[1], P.N. Yushmanov[1], T. Tajima[1,2], E.V. Belova[3], Z. Lin[2], W. Wang[2] and X. Wei[2]

[1] TAE Technologies, Inc., Foothill Ranch, CA 92610, United States of America
[2] University of California, Irvine, CA 92697, United States of America
[3] Princeton Plasma Physics Laboratory, Princeton, NJ 08540, United States of America

E-mail: sean@tae.com

Received 30 May 2021, revised 20 July 2021
Accepted for publication 17 August 2021
Published 15 October 2021

Abstract

The advanced beam-driven FRC is a field reversed configuration (FRC) with the addition of neutral beam (NB) injection, electrode biasing, and magnetic expander divertors. The resulting configuration has novel features that make it necessary to revisit many key results in FRC theory. Three of these features include (i) a large energetic ion population, (ii) in-principle capability to adjust the electric field and rotation profiles, and (iii) a combination of magnetic and electrostatic confinement of electrons in the SOL. In some fueling scenarios the electron density profile may exhibit a significant peak outside of the separatrix. To explore these features a hybrid fluid/kinetic equilibrium model has been used to reconstruct typical experimental profiles of the C-2W experiment. Results indicate that the energetic ions provide at least 50% of the total plasma pressure. These equilibrium profiles have been used as initial conditions for global, cross-separatrix, turbulent transport simulations using the 3D electrostatic particle-in-cell code ANC. Electrostatic fluctuations were found to nonlinearly saturate at an amplitude which is an order magnitude lower than that observed previously. The tokamak turbulence code GTC code has also been extended to handle FRC physics in the new GTC-X version, which has been used to perform simulations of turbulent transport in the SOL relevant to electrode biasing. It is found that equilibrium $E \times B$ flow shear significantly decreases ion temperature gradient saturation amplitude and ion heat transport. Also in the SOL, a 1D2V continuum code has been developed and applied to parallel electron heat transport. Results show the formation of pre-sheath potential and reduction of parallel electron heat loss close to the ideal ambipolar limit, a result which has been validated by experimental diagnostics. These transport modifications caused by the three novel configuration features help to explain the remarkable plasma performance of the C-2W experiment.

Keywords: field reversed configuration, equilibrium, transport, fast ions, open systems

(Some figures may appear in colour only in the online journal)

* Author to whom any correspondence should be addressed.

 © 2021 IAEA, Vienna Printed in the UK

1. Introduction

The FRC has been explored in many experimental facilities [1, 2]. It is of great interest as a fusion reactor concept due to its compact nature, high power density (typical average $\beta \sim 90\%$), axisymmetric geometry with simple circular confinement coils, and linear unrestricted divertor which can facilitate power, ash, and impurity removal. It has traditionally been considered a candidate geometry for aneutronic advanced fuels, such as the p-B11 reaction, which has recently been reassessed for magnetic confinement devices [3].

The advanced beam-driven FRC concept has been developed at TAE Technologies, Inc. over the last 20 years in the C-1 [4], C-2 [5, 6], C-2U [7, 8], and C-2W (aka 'Norman') [9] series of experimental devices, with concurrent development of simulation capability. During this period, TAE designed, built, and performed research on three completely new fusion plasma experiments (C-1, C-2, and C-2W) and one substantial upgrade (the C-2U upgrade to C-2). The C-2W experiment has achieved steady-state beam-driven FRC plasmas dominated by fast-ion pressure (>3 keV total temperature), with high electron temperature ($T_e > 500$ eV), 30 ms sustained FRC plasma, and demonstration of magnetic field ramp-up [9]. The layout of C-2W is sketched in figure 1. As indicated in the figure, the FRC plasma is confined in a region which includes true magnetic nulls at the O-point and at the two X-points. The poloidal magnetic field reversal and closed magnetic geometry are provided by diamagnetic current, which typically peaks around the separatrix. The ion orbits are comparable in size to the FRC and many are betatron orbits rather than drift orbits. The neutral beam injection, electrode biasing, and expander divertors are indicated as features (*a*), (*e*), and (*d*) in figure 1. The SOL flows along the axis through a magnetic mirror into a field expander divertor. See [10] in these proceedings for more details.

2. Equilibrium

Equilibrium of the FRC is studied with several models including one which allows multiple ion species with strong toroidal ion rotation (LR) [11]. This has recently been coupled to a fast ion Monte Carlo code (MC) [12] which models the NB injected fast ions, to create a hybrid fluid/kinetic equilibrium model (MC + LR) which can accommodate a significant (>50%) fast-ion current component. It is found that the separatrix shape is influenced by a combination of external magnetic field shaping, the ratio of edge pressure to O-point pressure, and the degree of anisotropy of the energetic ion population.

For C-2W a self-consistent equilibrium is obtained by performing an iterative process between MC and LR to arrive at a converged steady-state FRC equilibrium with fast ions. In order to reach steady conditions, the source (ionization of the injected neutral beam) is balanced by an artificial sink. For this purpose, an elevated neutral background density is used, giving rise to fast-ion losses by charge-exchange. The initial thermal FRC equilibrium is chosen based on experimental measurements such as Thomson scattering and magnetics data (the vacuum magnetic field is modeled using the experimental coil data). The converged FRC equilibria from the MC + LR code show good agreement with the experiments with main features like strongly-peaked electron density near the separatrix and the halo density outside the scrape off layer. A density peak in the scrape-off layer (SOL) is only possible with effective end confinement in the open-field plasma. Evidence was presented elsewhere [13] for mirror-like confinement, regulated by ion-scattering rather than free-streaming. This allows an elevated density layer to build up in the SOL in the presence of edge fueling by gas injection. Such edge-peaked density profiles have been routinely measured by Thomson scattering over hundreds of shots on the experiment where edge fueling has been used [10].

Simulation results helped to shed light on some features inaccessible by direct experimental measurements, such as current density profile and fast-ion current contribution. In particular C-2W reconstruction showed broad current density profiles with a gradient scale length on the order of fast ion gyro-radius, and a fast-ion current comparable to or exceeding that of the thermal plasma.

As an example, we show in figure 2 the MC + LR reconstruction of C-2W shot 119701 late in the discharge at time 20 ms. It was assumed that wall eddy currents have decayed by this time so that external magnetic field is provided only by the coils, with Greens' function method used to couple exterior/interior poloidal flux at the vacuum/plasma boundary. Neutral beams were operating at 6 MW, with the three main energy components (15 keV, 7.5 keV and 5 keV) that are created by initial ionization of gas in the beam system. Beams were assumed to have hydrogen species, while background thermal ions were deuterium. This is a typical operation scenario for C-2W though good plasmas can be obtained with either D or H thermal plasma. D beams may also be used for diagnostic purposes, but the majority of beams are fueled with H to avoid generating neutrons from beam-thermal D–D fusion. In the present equilibrium both thermal ions and electrons rotate. The separatrix radius is found to be $r_s = 31$ cm while the excluded flux radius, which is an experimental-analysis proxy for the separatrix radius, is $r_{\Delta\phi} = 35$ cm. (In hybrid FRCs with significant fast ion fraction it is typical for excluded flux radius to be larger than the separatrix radius [14].) Other parameters of the final equilibrium are: total current $I_{tot} = 190$ kAmp, fast ion current $I_{fast} = 110$ kAmp, midplane electron temperature at O-point $T_{Oe} = 190$ eV, midplane thermal-ion temperature at O-point $T_{Oi} = 330$ eV. The reconstructed equilibrium matches all key aspects of experiments, in particular, (1) magnetic flux and magnetic field measurements along the wall for both vacuum shot and plasma shots, (2) neutral beam shine-through, which was found to be 18%, equal to the experimental value measured by SEE detectors; (3) the midplane electron temperature profile from Thomson scattering, and (4) midplane electron density profile from Thomson scattering diagnostic. The density peak outside the separatrix is consistent with experimental observations for shot 119701 which had edge fueling by gas injection. This equilibrium reconstruction may be compared with the experimental results of [10].

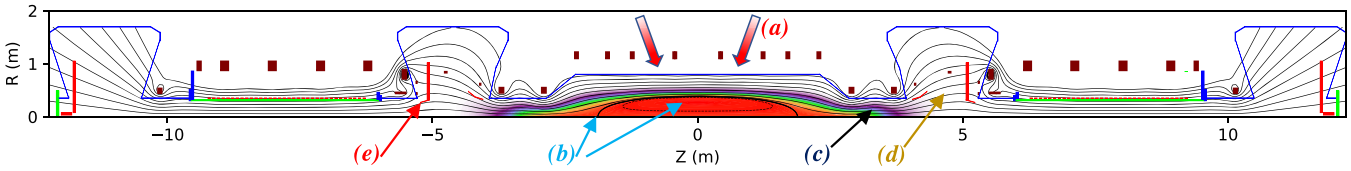

Figure 1. Sketch of the C-2W device in cylindrical section. Thin black lines are magnetic field lines, with the thicker black line denoting the separatrix. Arrows at (*a*) indicates the direction of neutral beam (NB) injection. Regions of null magnetic field at the O-point and X-points are indicated by (*b*). A magnetic mirror is shown at (*c*). One of the magnetic field expander divertors is indicated by (*d*). Red lines such as (*e*) indicate electrodes used for biasing.

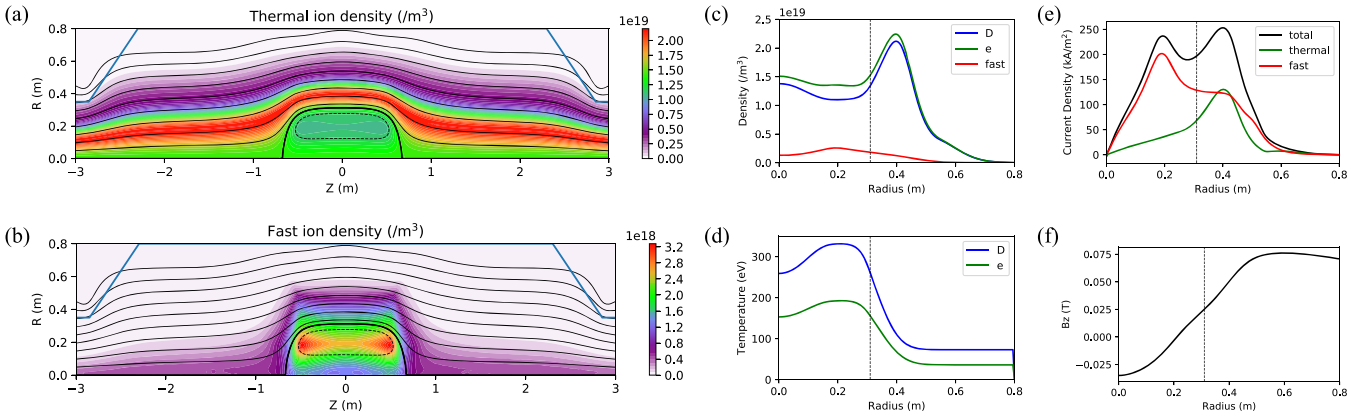

Figure 2. Shot 119701 MC + LR reconstruction equilibrium profiles. The left plots show (*a*) the 2D contours of thermal ion and (*b*) fast ion density. In both plots the black contours are contours of poloidal flux, with the thicker contour representing the separatrix. The right plots show midplane radial profiles of: (*c*) electron (green line), thermal D ion (blue) and fast ion density (red); (*d*) electron (green) and thermal D ion (blue) temperatures; (*e*) total current density (black), thermal plasma current density (green) and fast ion current density (red); and (*f*) magnetic field, B_z (T). In plots (*c*)–(*f*) the separatrix radius is indicated by the dashed vertical line.

The above method for equilibrium reconstruction is fairly labor intensive, but it captures the energetic ion component and the details of the experimental density and temperature profiles, which are needed for simulations of perpendicular turbulent transport in section 3.1 below. More rapid equilibrium reconstruction methods which do not include fast ion physics have also been developed using Bayesian inference methods [15] and a reduced physics model [16].

3. Transport

3.1. Perpendicular transport

Global confinement in macroscopically stable FRC plasmas is due to a combination of perpendicular confinement by magnetic field inside the separatrix, and parallel confinement by magnetic field gradients and electric fields in the SOL. The perpendicular and parallel transport are coupled [13].

Perpendicular turbulent transport is modeled using the 3D PIC codes ANC [17, 18], GTC [19] and GTC-X [20]. In previous simulations [20–22], a gyrokinetic particle push was used, necessitating the removal of magnetic null regions from the simulation domain. Nevertheless, nonlinear simulations find qualitative agreement in fluctuation spectrum with experimental Doppler back scattering (DBS) measurements [23]. To correctly include the magnetic null regions in global simulations, which entail a significant fraction of figure-8 and betatron orbits, a 'blended' drift-Lorentz particle pusher [24] without requirement of gyrokinetic validity has recently been implemented in ANC, and a corresponding δf model has been developed and applied [18]. Using this new particle model, linear and nonlinear results are found to be consistent with the previous gyrokinetic simulations. The new turbulence simulations also include kinetic electron effects which were neglected in the global gyrokinetic simulations [20, 22] but kept in local simulations [21].

In the ANC code electrons, ions, and beam ions were initialized with conditions from an equilibrium based on shot 119739, one of a series of shots with DBS measurements. In contrast with equilibria of previous studies, this equilibrium exhibits a density peak outside of the separatrix with temperature peaks inside, resulting in large $\eta_{\mathrm{i,e}}(\equiv L_{T_{\mathrm{i,e}}}^{-1}/L_n^{-1})$ which can excite microinstabilities potentially different than before (here L_n and $L_{T\mathrm{i,e}}$ are the scale lengths of density and ion or electron temperature). In these simulations, instability grows in the SOL as seen in figure 3(*b*). It is driven by the electron-temperature gradient, consistent with local simulations which included drift-kinetic electrons [21]. The excited mode also develops at faster time-scales on the order of microseconds, fast enough to be appropriate with the rapid response of fluctuations to profile changes seen in experiment. As seen in figures 3(*b*) and (*c*), the toroidal wavenumbers, defined as $k_\zeta \equiv \frac{n}{R}$, can differ significantly from the core to the SOL purely due to distance from the machine axis. The toroidal

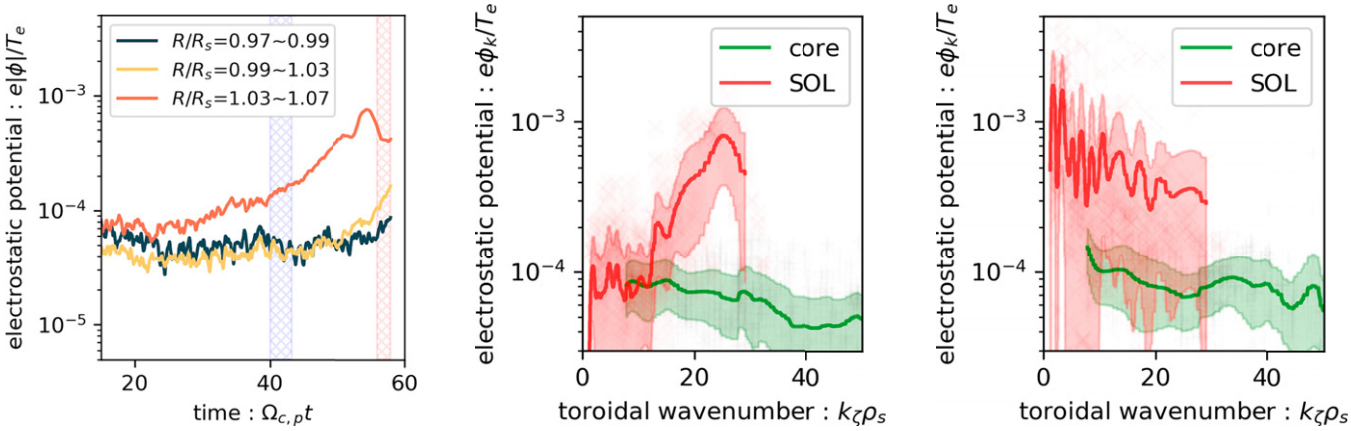

(a) Electrostatic fluctuation time history (b) Linear fluctuation spectrum (c) Nonlinear fluctuation spectrum

Figure 3. (*a*) Time histories of the electrostatic fluctuation RMS values inside, outside, and at the separatrix at the midplane. (*b*) Electrostatic fluctuation spectrum calculated during the linear growth phase which corresponds to the blue shaded region in (*a*). (*c*) Electrostatic fluctuation spectrum calculated during the nonlinearly saturated phase which corresponds to the red shaded region in (*a*). The lines in (*b*) and (*c*) depict a moving average while the shaded regions depict the standard deviation about the moving average.

wavenumbers are normalized such that wavelengths are 'short' (wavenumbers are 'large') relative to the local ion sound gyroradius, defined as $\rho_s \equiv \frac{\sqrt{T_e m_i}}{eB}$.

While the linear properties of the instabilities may differ from the C2/C2U simulations [20–22], the overall evolution of fluctuations, depicted in figure 3, remains similar. Consistent with previous simulations, the FRC core is found to be inherently stable while short toroidal wavelength ($k_\zeta \rho_{se} \sim 20.15$) instabilities grow in the SOL. As the instability saturates, energy cascades from short to long wavelengths in the SOL and fluctuations originating from the SOL spread into the core. Differing from the previous work, the fluctuations saturate at lower levels, $e\,|\phi|\,/T_e \sim \mathcal{O}(10^{-3})$ compared with $e\,|\phi|\,/T_e \sim \mathcal{O}(10^{-2})$, and the spread of fluctuations into the core is much weaker than prior. These differences may be due to several possible mechanism, including but not limited to a stabilizing influence of fast 'beam' ions which were previously neglected, a stabilizing influence of large thermal-ion orbits from the more realistic particle model, or the change in the nature of the linear instability. Preliminary results from ongoing analysis suggest that, while the underlying linear mechanism is kinetic in nature, electron heat transport appears to be a fluid-like process with conductivity comparable to a diffusive process related to the correlation length and eddy rotation time, i.e. $\chi_e \sim \frac{\lambda_{corr}^2}{\tau_{eddy}}$.

In the SOL, GTC-X simulations find that equilibrium $E \times B$ flow shear significantly decreases ion temperature gradient (ITG) saturation amplitude and ion thermal transport by reducing both turbulence intensity and eddy size [25]. Further simulations find that the ion thermal transport decreases with lower collisional damping of the self-generated zonal flows, which have no collisionless damping in the ideal FRC [26]. See [27] in these proceedings for more details.

3.2. Parallel electron transport

A combination of magnetic and electrostatic confinement has been employed in C-2W to improve the electron parallel confinement. In an expander divertor the magnetic field strength drops significantly between a magnetic mirror and the target wall as can be seen in figure 1. The electron pressure drops with the magnetic field, leading to the development of a pre-sheath, and the drop of potential in this pre-sheath reduces the potential drop in the sheath itself. In addition, lower plasma density near target walls causes increase of the Debye length which further decreases surface electric field. The favorable role of the expander has been demonstrated in the gas dynamic trap (GDT) experiment, where electron temperature has been enhanced to 800 eV by ECRH and neutral beams in the presence of magnetic expander divertor [28–30], and in the C-2W experiment, where electron temperature has been enhanced to 500 eV [10]. (The physics of the parallel electron transport in these two devices is expected to be very similar, but the development goals of the two concepts are different as GDT is currently being explored as a neutron source [31] while the advanced FRC, with its high β and, consequently, high potential fusion power output, is being explored as a fusion reactor for electricity production.)

Parallel electron heat transport in the SOL has been modeled using a custom developed 1D2V Vlasov Fokker Planck code with full collisional operator with open spatial boundary conditions and Poisson solver [32]. A half-Maxwellian distribution is injected into the magnetic expander and an outflow boundary condition is imposed on the particles reflected back from the electrostatic barrier. At the cold end i.e. electrodes, the logical sheath boundary condition [33] is used. As expected, simulations show the formation of a pre-sheath potential, and consequently the parallel electron heat losses are

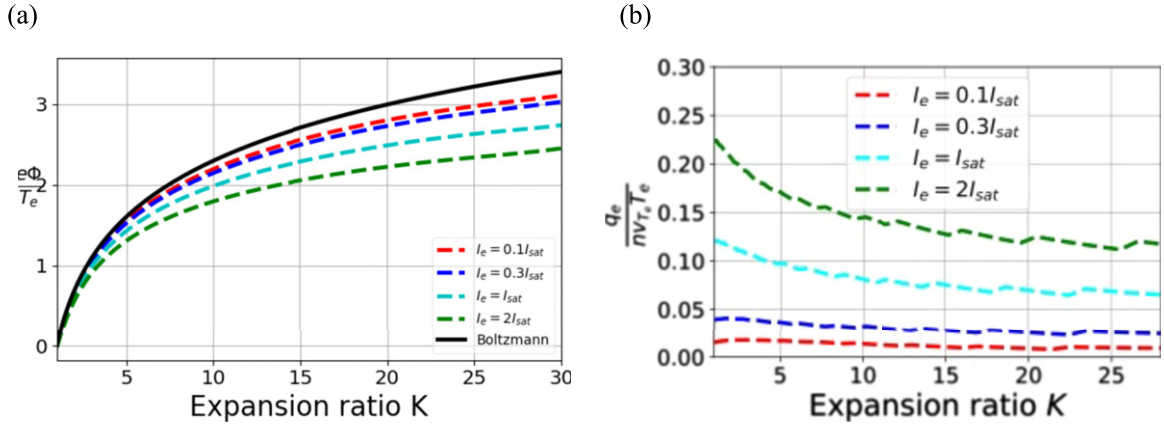

Figure 4. (*a*) Electrostatic potential profiles decreases with increasing electron losses. (Vertical axis has reversed sign.) (*b*) Heat flux decreases with increasing magnetic expansion (K) and decreasing electron losses/current I_e. Expansion ratio K parameterizes the distance from the magnetic mirror along the field line.

reduced to a level close to the minimal theoretical limit. This result has been validated [34] by experimental measurements (see also [10]).

Kinetic calculations show that the pre-sheath electrostatic potential drop in the magnetic expander region (figure 4(*a*)) decreases with increased electron losses to the walls. These results can be qualitatively explained using the electron axial pressure balance equation

$$\frac{\mathrm{d}P_\parallel}{\mathrm{d}l} + \left(P_\perp - P_\parallel\right)\frac{\mathrm{d}\ln B}{\mathrm{d}l} + en\frac{\mathrm{d}\phi}{\mathrm{d}l} = 0,$$

where $P_\parallel = nT_\parallel$ is the parallel electron pressure, $P_\perp = nT_\perp$ is the perpendicular electron pressure, n is electron density, B is the magnetic field, and ϕ is the electrostatic potential. The asymptotic theory result (black line in figure 4(*a*)) is recovered with $I_e = 0$, i.e. with no electron losses. In this limit the distribution is isotropic i.e. $T_\perp \approx T_\parallel \approx$ const., and hence the potential reduces to the Boltzmann potential. With increasing electron losses (I_e), temperature anisotropy increases as the reflected distribution is truncated and the trapped region between the sheath boundary and the mirror boundary is never filled up completely by collisions. With temperature anisotropy, $P_\parallel > P_\perp$, which leads to a reduction in potential compared to the Boltzmann potential. The heat flux ($q_e = \int\int \frac{v_\parallel^2}{2} v_\parallel f\, \mathrm{d}^3v$) profile is shown in figure 4(*b*) for various electron losses/current I_e values and it is found to decrease with increasing expansion ratio $K = B_m/B$ (B_m is field under the mirror), as electron thermal energy is converted to potential energy. Also, heat flux decreases with decreasing electron losses or current (i.e. I_e). In the figure, electron current values less than the ion saturation current, $I_e < I_{sat}$, correspond to negative biasing on the electrode and electron current values $I_e > I_{sat}$ correspond to positive biasing. Therefore, negative biasing is associated with reduced electron heat transport.

4. Summary

Novel features brought by the several innovations of the advanced beam-driven FRC plasmas have stimulated further development of equilibrium and transport models. A hybrid fluid/kinetic equilibrium model is able to reproduce C-2W experimental diagnostics, which leads to a force-balanced equilibrium reconstruction where 50% of the total plasma current is in the fast ion population generated by the neutral beams. Global, 3D, cross-separatrix, nonlinear, electrostatic turbulent transport simulations show that the new equilibrium features reduce the non-linear saturation amplitude of electrostatic fluctuations. 3D simulations in the SOL find that equilibrium $E \times B$ flow shear significantly decreases ITG saturation amplitude and ion heat transport. 1D2V continuum modeling of electron dynamics in the SOL shows that parallel electron thermal loss decreases with increasing divertor expansion ratio and also is also decreased by negative biasing on the central electrode. These theoretically predicted changes in equilibrium and transport characteristics may help to explain the remarkable plasma performance of the C-2W experiment.

Acknowledgments

The authors would like to thank the TAE team at TAE Technologies, Inc. for operations and experimental measurements which form the foundation this research is built upon. Part of the work was funded by TAE Technologies, Inc. The research used resources of the United States Department of Energy Office of Science (US DOE SC) and Fusion Energy Sciences (FES). Part of the work was funded under the INFUSE program—a DOE SC FES private-public partnership—under CRADA No. 2703 between Princeton Plasma Physics Laboratory and TAE Technologies, Inc. The research used the resources of the National Energy Research Scientific Computing Center (NERSC), a US DOE SC User Facility located at Lawrence Berkeley National Laboratory supported under Contract No. DE-AC02-05CH11231, and Argonne Leadership Computing Facility (ALCF), a US DOE SC User Facility at Argonne National Laboratory supported under Contract No. DE-AC02-06CH11357. Awards of computer time were provided by the Innovative and Novel Computational Impact on Theory and Experiment (INCITE)

program and by the ASCR (Advanced Scientific Computing Research) Leadership Computing Challenge (ALCC) program. In addition, the authors acknowledge suggestions and improvements, specifically the 'blended' particle pusher and the ADIOS2 I/O framework provided through collaboration with members of the US DOE Exascale Computing Project (ECP) which is a partnership between the US DOE SC and the US DOE National Nuclear Security Administration.

ORCID iDs

S.A. Dettrick https://orcid.org/0000-0002-1756-4625
D.C. Barnes https://orcid.org/0000-0002-0111-1621
F. Ceccherini https://orcid.org/0000-0003-3377-6932
L. Galeotti https://orcid.org/0000-0003-3426-2087
S.A. Galkin https://orcid.org/0000-0002-1670-7364
S. Gupta https://orcid.org/0000-0001-5688-4122
O. Koshkarov https://orcid.org/0000-0002-0935-760X
C.K. Lau https://orcid.org/0000-0001-6702-1461
A. Necas https://orcid.org/0000-0002-9054-7653
B.S. Nicks https://orcid.org/0000-0002-3876-8299
M. Onofri https://orcid.org/0000-0003-0818-4628
L.C. Steinhauer https://orcid.org/0000-0003-2227-7345
K. Yakymenko https://orcid.org/0000-0002-7663-8006
E.V. Belova https://orcid.org/0000-0002-1525-1027
Z. Lin https://orcid.org/0000-0003-2007-8983
W. Wang https://orcid.org/0000-0001-8743-0430
X. Wei https://orcid.org/0000-0001-7486-0407

References

[1] Tuszewski M. 1988 Field reversed configurations *Nucl. Fusion* **28** 2033
[2] Steinhauer L.C. 2011 Review of field-reversed configurations *Phys. Plasmas* **18** 070501
[3] Putvinski S.V., Ryutov D.D. and Yushmanov P.N. 2019 Fusion reactivity of the pB11 plasma revisited *Nucl. Fusion* **59** 076018
[4] Rostoker Norman, Binderbauer Michl, Garate Eusebio and Bystritskii Vitaly 2005 Formation of a field reversed configuration for magnetic and electrostatic confinement of plasma *Report* US6891911B2
[5] Binderbauer M.W. *et al* 2010 Dynamic formation of a hot field reversed configuration with improved confinement by supersonic merging of two colliding high-β compact toroids *Phys. Rev. Lett.* **105** 045003
[6] Tuszewski M. *et al* 2012 A new high performance field reversed configuration operating regime in the C-2 device *Phys. Plasmas* **19** 056108
[7] Binderbauer M.W. *et al* 2015 A high performance field-reversed configuration *Phys. Plasmas* **22** 056110
[8] Guo H.Y. *et al* 2015 Achieving a long-lived high-beta plasma state by energetic beam injection *Nat. Commun.* **6** 6897
[9] Gota H. *et al* 2019 Formation of hot, stable, long-lived field-reversed configuration plasmas on the C-2W device *Nucl. Fusion* **59** 112009
[10] Gota H. *et al* 2021 Overview of C-2W: high temperature, steady-state beam-driven field-reversed configuration plasmas *Nucl. Fusion* (submitted)
[11] Galeotti L., Barnes D.C., Ceccherini F. and Pegoraro F. 2011 Plasma equilibria with multiple ion species: equations and algorithm *Phys. Plasmas* **18** 082509
[12] Dettrick S., *et al* 2012 Monte Carlo simulation of neutral beam injection in C2 *Advanced Controls and Diagnostics for Confinement Improvement of Compact Toroids US-Japan Compact Torus Workshop, CT 2012* (Newport Beach, California, USA, 25–28 September 2012)
[13] Steinhauer L.C. and Berk H.L. 2018 Coupled transport in field-reversed configurations *Phys. Plasmas* **25** 022503
[14] Tuszewski M., Gupta D., Gupta S., Onofri M., Osin D., Deng B.H., Dettrick S.A., Hubbard K. and Gota H. 2017 Equilibrium properties of hybrid field reversed configurations *Phys. Plasmas* **24** 012502
[15] Romero J.A., Dettrick S.A., Granstedt E., Roche T. and Mok Y. 2018 Inference of field reversed configuration topology and dynamics during Alfvenic transients *Nat. Commun.* **9** 691
[16] Steinhauer L.C., Roche T. and Steinhauer J.D. 2020 Anatomy of a field-reversed configuration *Phys. Plasmas* **27** 112508
[17] Fulton D.P., Lau C.K., Schmitz L., Holod I., Lin Z., Tajima T. and Binderbauer M.W. (TAE Team) 2016 Gyrokinetic simulation of driftwave instability in field-reversed configuration *Phys. Plasmas* **23** 056111
[18] Lau C.K., Fulton D.P., Bao J., Lin Z., Dettrick S., Binderbauer M., Tajima T. and Schmitz L. 2020 Electrostatic quasi-neutral formulation of global cross-separatrix particle simulation in field-reversed configuration geometry *Phys. Plasmas* **27** 082504
[19] Lin Z., Hahm T.S., Lee W.W., Tang W.M. and White R.B. 1998 *Science* **281** 1835
[20] Bao J., Lau C.K., Lin Z., Wang H.Y., Fulton D.P., Dettrick S. and Tajima T. 2019 Global simulation of ion temperature gradient instabilities in a field-reversed configuration *Phys. Plasmas* **26** 042506
[21] Lau C.K., Fulton D.P., Holod I., Lin Z., Binderbauer M., Tajima T. and Schmitz L. 2017 Drift-wave stability in the field-reversed configuration *Phys. Plasmas* **24** 082512
[22] Lau C.K., Fulton D.P., Bao J., Lin Z., Tajima T., Schmitz L. and Dettrick S. 2019 Cross-separatrix simulations of turbulent transport in the field-reversed configuration *Nucl. Fusion* **59** 066018
[23] Schmitz L. *et al* 2016 Suppressed ion-scale turbulence in a hot high-β plasma *Nat. Commun.* **7** 13860
[24] Cohen R.H., Friedman A., Grote D.P. and Vay J.-L. 2007 Large-timestep mover for particle simulations of arbitrarily magnetized species *Nucl. Instrum. Methods Phys. Res.* A **577** 52–7
[25] Wang W. *et al* 2021 Effects of equilibrium radial electric field on ion temperature gradient instability in the scrape-off layer of a field-reversed configuration *Plasma Phys. Control. Fusion* **63** 065001
[26] Wei X.S., Wang W.H., Lin Z., Choi G.J., Dettrick S., Lau C., Liu P.F. and Tajima T 2021 Effects of zonal flows on ion temperature gradient instability in the scrape-off layer of a field-reversed configuration *Nucl. Fusion* (submitted)
[27] Lin Z. 2021 Verification and validation of particle simulation of turbulent transport in FRC *International Atomic Energy Agency Fusion Energy Conference Fusion Energy Conf. Proc. 28th Int. Conf.* (virtual conference, 10-15th May 2021) (Vienna: IAEA) paper TH/P7-1
[28] Soldatkina E., Anikeev M., Bagryansky P., Korzhavina M., Maximov V., Savkin V., Yakovlev D., Yushmanov P. and Dunaevsky A. 2017 Influence of the magnetic field expansion on the core plasma in an axisymmetric mirror trap *Phys. Plasmas* **24** 022505
[29] Bagryansky P.A., Shalashov A.G., Gospodchikov E.D., Lizunov A.A., Maximov V.V., Prikhodko V.V., Soldatkina E.I., Solomakhin A.L. and Yakovlev D.V. 2015 Threefold increase of the bulk electron temperature of plasma discharges in a magnetic mirror device *Phys. Rev. Lett.* **114** 205001

[30] Ivanov A.A., Burdakov A.V. and Bagryansky P.A. 2015 Recent progress in studies of plasma heating and stabilization in axisymmetric magnetic mirrors in Novosibirsk *Fusion Sci. Technol.* **68** 56–62

[31] Ivanov A.A. and Prikhodko V.V. 2013 Gas-dynamic trap: an overview of the concept and experimental results *Plasma Phys. Control. Fusion* **55** 063001

[32] Gupta S., Yushmanov P. and Barnes D.C. 2017 Vlasov Fokker Planck study of electron dynamics in the scrape off layer with expander divertor *59th Annual Meeting of the APS Division of Plasma Physics* (Milwaukee, Wisconsin, 23–27 October 2017) (American Physical Society) vol 62 https://meetings.aps.org/Meeting/DPP17/Event/308723

[33] Parker S.E., Procassini R.J., Birdsall C.K. and Cohen B.I. 1993 A suitable boundary condition for bounded plasma simulation without sheath resolution *J. Comput. Phys.* **104** 41–9

[34] Griswold M and Yushmanov P 2019 Measurement of axial plasma losses in the C-2W high-performance regime *61st Annual Meeting of the APS Division of Plasma Physics* (Fort Lauderdale, Florida, USA, 21–25 October 2019) http://meetings.aps.org/link/BAPS.2019.DPP.UP10.140